Original Research Articles

Climate Sensitivity Parameter in the Test of the Mount Pinatubo Eruption

ABSTRACT

The author has developed one dimensional dynamic model (1DDM) to simulate the surface temperature change (ΔT) caused by the eruption of Mount Pinatubo. The main objectives have been 1) to test the climate sensitivity parameter (λ) values of 0.27 K/(Wm^{-2}) and 0.5 K/(Wm^{-2}), 2) to test the time constants of a simple first-order dynamic model, and 3) to estimate and to test the downward longwave radiation anomaly (ΔLWDN). The simulations show that the calculated ΔT of 1DDM follows very accurately the real temperature change rate. This confirms that theoretically calculated time constants of earlier studies for the ocean (2.74 months) and for the land (1.04 months) are accurate and applicable in the dynamic analyses. The 1DDM-predicted ΔT values are close to the measured value, if the λ-value of 0.27 K/(Wm^{-2}) has been applied but the λ-value of 0.5 K/(Wm^{-2}) gives ΔT values, which are about 100 % too large in the early phases of the eruption. The main uncertainty in the Mount Pinatubo analyses is the ΔLWDN flux, because there are no direct measurements available during the eruption. The author has used the measured ERBS fluxes and has also estimated ΔLWDN flux using the apparent transmission measurements. This estimate gives the best and most consistent results in the simulation. A simple analysis shows that two earlier simulations utilising General Circulation Models (GCM) by two research group are depending on the flux value choices as well as the measured ΔT choices. If the commonly used minimum value of -6 Wm^{-2} would have been used for the shortwave anomaly in the GCM simulations, instead of -4 Wm^{-2}, the ΔT values would differ from the measured ΔT values almost 100 %. The main reason for this error seems be the λ-value of 0.5 K/(Wm^{-2}). The mean λ-value of 1.0 K/(Wm^{-2}) commonly used in GCMs would give 200 % too high values.

Keywords: Global warming, climate sensitivity parameter, climate response time, radiative forcing response, downward radiative fluxes, Mount Pinatubo eruption.

1. INTRODUCTION

1.1 Objectives and Symbols

The Mount Pinatubo eruption in 1991 caused a global cooling during the next five years as the incoming shortwave radiation was reduced by 6 W/m^2 offering a unique opportunity to test and to analyse the various phenomenon of the climate system. The first objective of this paper is to test the two climate sensitivity parameter values which have been commonly used in the scientific studies. The second objective is to test the climate system time constants describing the dynamic behaviour of the climate exposed to a relative big and sudden change. The third objective is to estimate and to test the downward longwave radiation anomaly (ΔLWDN). In the simulations a theoretical feedback property of the climate system has been also tested.

Table 1 includes all the symbols, abbreviations, acronyms and definitions used repeatedly in this paper.

Table 1. List of symbols, abbreviations, and acronyms

Acronym	Definition
1DDM	One dimensional dynamic model
AT	Apparent transmission
ENSO	El Niño Southern Oscillation
ERBS	NASA's Earth Radiation Budget Satellite
ECS	Equilibrium climate sensitivity
GCM	General Circulation Model
ISCCP	International Satellite Cloud Climatology Project
LW	Longwave
LWDN	LW radiation flux downward
LWUP	LW radiation flux upward
LWSRF	LW radiation emitted by the surface
ONI	Oceanic Niño Index
RF	Radiative forcing change
SW	Shortwave
SWATM	SW radiation flux absorbed by the atmosphere
SWIN	SW radiation flux incoming at the TOA
SWSRF	SW radiation flux incoming at the surface
TOA	Top of the atmosphere
TPW	Total precipitable water
T	Surface temperature
Tm	1DDM-predicted surface temperature change
Tav	Average surface temperature by four datasets
Tmsu	Surface temperature by UAH MSU dataset
Tav-e	Tav with ENSO correction
Tmsu-e	Tmsu with ENSO correction
TCS	Transient climate sensitivity
λ	Climate sensitivity parameter
Δ	Anomaly or change

Subscript_n means step n in time domain.

1.2 The Mount Pinatubo eruption

The main eruption of the Mount Pinatubo volcano (15.1 °N, 120.3 °E) on the island of Luton in the Philippines began on the 3rd of June, 1991 and concluded on the next day. Four large explosions generated eruption columns reaching the heights of up to 24 km in the stratosphere. The estimate of the stratospheric mass increase was 14 – 20 Mt of SO_2, which created 21-40 Mt of H_2SO_4–H_2O aerosols [1]. The eruption also injected vast quantities of minerals and metals into the troposphere and stratosphere in the form of ash particles. The aerosols formed a global layer of sulfuric acid haze over the globe and the global temperatures dropped about 0.5 °C in the years 1991 – 1993.

The sulphate aerosols caused scattering of the visible light and therefore the incoming radiation scattered more effectively back into space. Thus the albedo of the Earth increased leading to a cooling at the Earth's surface. On the other hand the plants utilized the climate conditions, because they could photosynthesize more effectively in the diffuse sunlight [2]-[3]. As a result of the more intensive photosynthesis, there was a negative anomaly of the global CO_2 concentration increase rate.

Because the eruption happened at one point, it took several weeks before the global effect was fully developed. The volcanic aerosol cloud encircled the Earth in 21 days driven by the easterly winds in the tropical stratosphere. It covered about 42 % of the Earth in two weeks [4]. In Fig. 1 are depicted the global temperature [5] and the apparent transmission measured at Mauna Loa [6] (19.3 °N, 155.4 °W). It can be seen that there is delay between the temperature response and the apparent transmission (AT) describing the reduction of the incoming shortwave (SW) radiation.

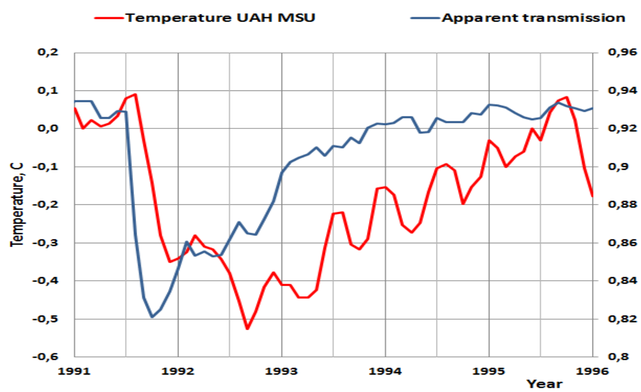

Fig.1. The global surface temperature and the apparent transmission measured at Mauna Loa, Hawaii.

In Fig. 2 the apparent transmissions (AT) are depicted at the various sites on the northern hemisphere [7]. It can be seen that the absolute values of the AT values are different depending mainly on the local conditions. For example, the low values of the Japanese sites describe the air quality of the local conditions. The large value of the Mauna Loa is due to the fact that it is at the altitude of 3.4 km in the middle of the Pacific. An important feature thinking the analysis methods of this study is that the percentage decreases are very close to each other in the range from 10.1 % to 13.2 %.

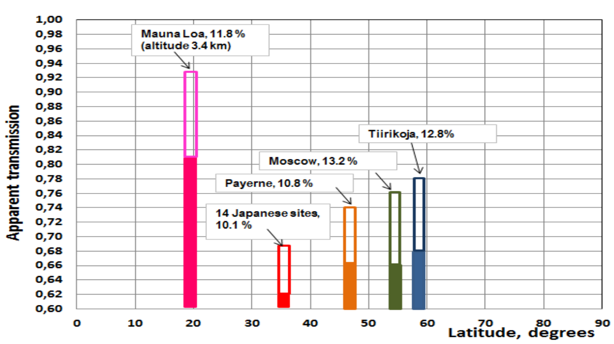

Fig. 2. The apparent transmission values at the various sites. The percentage values show the maximum decreases of the apparent transmissions after the eruption.

The sites in Fig. 2 cover almost 85 % of the northern hemisphere. It can be assumed that the same development happened on the southern hemisphere as well. The reason why the decrease of apparent transmission value is almost the same at the high latitudes as in the tropics is probably due to the zenith angle. Even though the sulphate cloud would be thinner at the high latitudes, the sunlight has a longer pathway through the atmosphere. This compensates the effects of thinner cloud conditions and causes finally the same decrease in the SW insolation flux.

Two conclusions can be drawn from these figures. The global delay called a dead time in process dynamics, is estimated to be 1.6 months between the incoming SW radiation change and the global surface temperature response. This value is used in the dynamical analyses of this study.

Another conclusion is that after the fully developed coverage of the sulphate cloud in the stratosphere, the radiation effect changes can be estimated to happen simultaneously over the globe. Therefore it is justified to use the one dimensional (1D) approach in developing a dynamic model (called 1DDM) for analysing the temperature versus radiation flux relationships.

1.3 Earlier studies

There have been numerous Pinatubo studies on the three major fields. The first is on the aerosol and chemical effects of the Pinatubo particles. The second is focused on optical properties of the aerosol particles and on the radiative forcing. The third is on the responses to the forcing affecting the temperature and the circulation patterns.

This paper concentrates on the dynamic behaviour of the surface temperature changes caused by the radiative flux changes. Therefore the survey of the earlier studies covers only the subjects which are relevant for this study.

Even though the Pinatubo eruption is the best documented major eruption so far, there was an essential radiative flux, which was not directly measured during the eruption. This was the LW downward radiation flux (LWDN), which is essential, because it compensates the major portion of the cooling effects of the reduced SW downward radiation flux (SWIN) decrease during the early phases of the eruption [8].

The World Climate Research Programme (WCRP) Radiative Fluxes Working Group initiated a new Baseline Surface Radiation Network (BSRN) to support the research projects. Some years later the BSRN was incorporated into the WCRP Global Energy and Water Cycle Experiment (GEWEX). The BSRN network stations started to operate in 1992 and that is why these valuable measurements were not available during the Pinatubo eruption. In October 2010 the Eyjafjallajökull volcano in Iceland erupted, covering the major part of Europe with the ash cloud. Strange enough – even though there were 10 operational BSRN stations in this area - none of them was measuring LWDN fluxes during the eruption. So another case was missed in detecting this essential radiative flux during a volcano eruption.

There has been a special GEWEX project to assess the surface radiation budget datasets [9] based on the available data at TOA. By studying the GEWEX results, the author's conclusion is that the LWDN fluxes could not be estimated reliably in this project based on the other existing flux data. Therefore a major challenge in this study is to estimate the ΔLWDN flux trend during the Pinatubo eruption.

In Fig. 3 the radiative fluxes of the Earth are illustrated [10]-[11]. The climate forcing effect of a volcano eruption can be analysed in the same way as the cloud change forcing. Normally the cloud forcing has been calculated as the sum of changes in the downward SW flux change and outgoing LW flux change between the clear and all-sky conditions. Applying this same method, the radiative forcing (RF) caused by the eruption, is the sum of ΔSWIN and ΔLWUP and it is called aerosol radiative forcing [12]. The change in the flux values is calculated between the normal conditions and during or after the eruption. Because the outgoing LW flux is reduced during the early phases of the eruption, it is a sign that there is cooling happening on the surface.

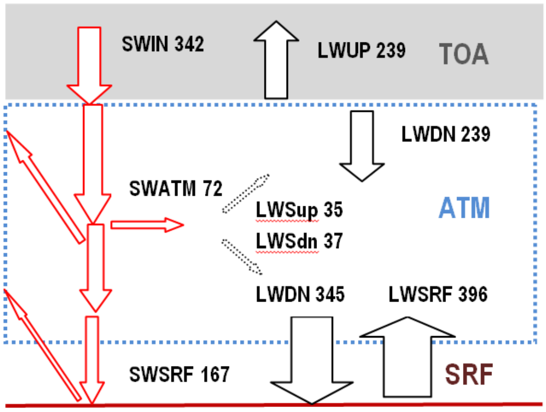

Fig. 3. The main radiative fluxes of the Earth's energy balance.

The RF value calculated in this way is normally called radiative or climate forcing (RF). Actually it is only a measure of the real RF. There are two fluxes which have the real forcing effect on the Earth's surface temperature (T) and they are SWIN and LWDN. In the case of cloudy sky and the all-sky, the change of LWUP is 11 Wm^{-2} and the change of LWDN is 14.3 Wm^{-2}, showing that the changes are not equal even though they are close to each other [11].

The small particle sizes less than 1 µm are more effective in reflecting the SW solar radiation SWIN than they are at reflecting the LW radiation emitted by the surface. According to a comprehensive study [1], the smallest particles were sulphuric acid/water droplets and the largest particles were ash fragments. The cooling and warming effects of the aerosols and particles depend on the particle sizes. The LWDN flux increases especially during the early phases of the eruption because there are larger aerosol particles more in the atmosphere than in the later phases. Therefore the warming effect of LWDN is the most effective at the same time as the cooling is in maximum [1]. The stratospheric ash layer settled down just above the troposphere staying there until March 1992. The particle size measurements [1] showed that there was a peak in both small and large particle sizes after a few months after the eruption but by 1993 the high measurements values were decaying back to pre-eruption values.

The ash cloud in the high altitudes of the atmosphere absorbs and emits radiation. This ash cloud had a measureable warming effect on the northern hemisphere winter temperatures [13]-[14]. The ash cloud has about the same effect as the clouds have in the cold climate conditions that it will prevent the cooling of the surface. In this way it has a net warming effect.

The forcing studies can be classified into two categories namely forcing calculations utilising General Circulation Models (GCM) 1) for simulations of spatial flux and temperature changes [12], [14]-[19], and 2) other simulations resulting the surface temperature change. In respect to this study only the latter studies are relevant.

One of the earliest studies was that of Hansen et al. [20]. They used the GISS global climate model to assess the preliminary impacts of the Pinatubo eruption. In their calculations they used the peak value of -4 Wm^{-2} for ΔSWIN and they could show that the simulated ΔT was about -0.5 °C. The most common value of ΔSWIN has been -6 Wm^{-2} [12]-[13], [16]-[17], [21]. This value is also used in this study.

In the later study [22] Hansen et al. applied the same peak value of -4 Wm^{-2} in the GCM simulations by name SI94 and GRL92. Soden et al. [23] applied a GCM and as input data they used ERBS fluxes in calculating the RF values. They also included the absolute atmospheric water content as a variable. The peak value of – 4 Wm^{-2} was used for ΔSWIN. Their major result was the GCM simulations could calculate the ΔTm values close to the measured value, if the positive water feedback was included. The water content was calculated using the NASA Water Vapor Project (NVAP) values [24]. In Fig. 4 the NVAP dataset values as well the NCEP/NCAR (National Center for Environmental Prediction / National Center for Atmospheric Research) values are depicted [25]. The graphs show that there are opposite trends in these datasets during the Pinatubo eruption. It is quite impossible to know, which of these datasets is correct and therefore the question of positive or negative water feedback cannot be reliably tested utilising the Pinatubo case.

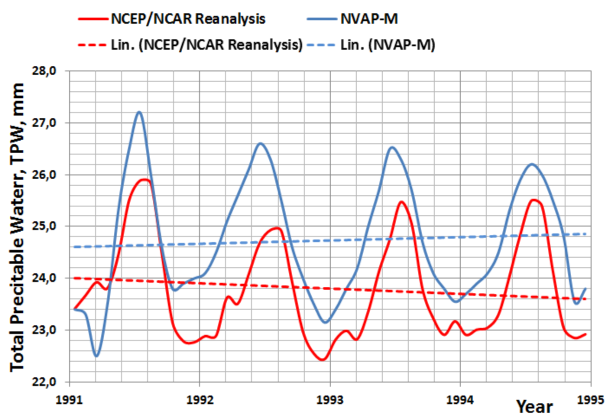

Fig. 4. The graphs of water contents according to NVAP-M and NCEP/NCAR datasets.

The radiative forcing (RF) at TOA has a linear relationship to the global mean surface temperature change ΔT, if the equilibrium state is assumed [26]:

$$\Delta T = \lambda RF, \quad (1)$$

where λ is the climate sensitivity parameter. According to IPCC [27] λ is a nearly invariant parameter having a value of 0.5 $K/(Wm^{-2})$. IPCC uses this value in calculating the transient climate sensitivity (TCS) value of 1.75 °C [26] (0.5 K/(Wm-2)* 3.7 Wm^{-2} = 1.75 K). Actually there should not be any of IPCC's own climate models, but in reality the structure and the values of such a model called "Radiative Forcing by Emissions and Drivers" has a summary leading to the value of 2.34 Wm^{-2} [28]. According to IPCC's own definition, the ΔT of this model should be 1.17 °C in 2011. IPCC does not show this temperature increase in the latest Assessment Report 5 and a reason might be that it is 38 % greater than the observed value.

Ollila has analysed [29] the future warming values based on the RF values of greenhouse gases. In these analyses of the different RCPs (Representative Concentration Pathways), IPCC uses the λ value of about 0.36 $K/(Wm^{-2})$. Thus it appears that IPCC is very inconsistent in using the λ.

IPCC has made a summary of 30 GCMs in the Assessment Report 5 (AR5). The λ values used in their summary vary between 0.6 and 1.6 totally in 23 GCMs and the model mean is 1.0 $K/(Wm^{-2})$. A so high λ should be used only in calculating the equilibrium climate sensitivity (ECS). EQS is roughly twice the value of TCS and it takes hundreds of years to reach the equilibrium state [28]. The TSC can be reached in less than a year, because the water feedback reacts very quickly to the temperature changes. The possible water feedback is the only essential feedback in TCS calculations. In the referred GCM studies applied in the Pinatubo analyses, there are no specifications about the λ value of these GCMs.

There are several studies, which have calculated the climate sensitivity value to be about 1.0 – 1.2 ℃ [30]-[33] using the same radiative forcing value of 3.7 Wm^{-2} for CO_2 as IPCC uses. It means a lower λ value of about 0.3 $K/(Wm^{-2})$. Some researchers have calculated even lower values like 0.6 ℃ for climate sensitivity [29], [34] or 0.7 ℃ [35]. Ollila [29] has calculated the λ value using three different methods and his results vary between 0.245 and 0.331 the most reliable value being 0.268 $K/(Wm^{-2})$. In this study these two most common values have been applied: 0.27 $K/(Wm^{-2})$ and 0.5 $K/(Wm^{-2})$.

2. RADIATIVE FLUXES AND FORCING ANOMALIES CAUSED BY THE ERUPTION

The two SWIN flux datasets available during the eruption are ISCCP [36] and ERBS [37]. They are depicted in Fig. 6. Both datasets are unstable and spiky. The SWIN flux anomaly can also be estimated using the apparent transmission (AT) signal or optical depth measurements. In this case the AT signal of Mauna Loa has been used. The ΔSWIN flux anomaly has been assumed to follow exactly the trend of the AT-signal. The time of the minimum value of the AT-signal has been used to be also the time of the minimum value of the SWIN flux value of -6 Wm^{-2}. This estimate of ΔSWIN flux is depicted in Fig. 5 and it can be noticed that this flux is very stable and its trend follows very well the average form of ISCCP and ERBS fluxes. The smoothed ΔERBS SWIN flux signal follows the estimated AT transformed ΔSWIN flux signal so well that they could be used between each other.

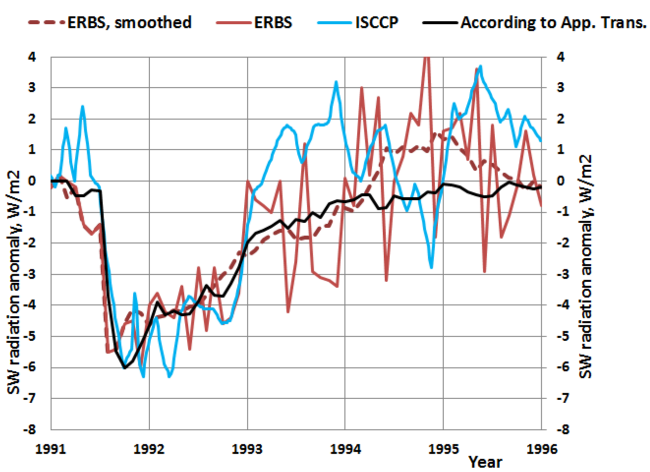

Fig. 5. SW downward radiation flux anomalies at TOA.

The two LWUP flux datasets available are ISCCP [36] and ERBS [37]. They are depicted in Fig. 6. Both fluxes are very spiky and the flux levels have the difference of about 1 Wm^{-2} after the year 1993.

Because there are no direct measurements of LWDN flux, it has been estimated. As realized before, the LWDN flux anomaly should follow the amount of large aerosol particle amounts in the atmosphere. Russell et al. has a Fig. 6 in their paper [1] containing information about the different particle size trends measured at Mauna Loa during the eruption.

It has been assumed that the smaller particle sizes from 0.382 to 0.500 µm are related to the ΔSWIN flux anomaly. The largest particle size is 1.020 µm and this graph has been used to estimate the ΔLWDN flux peak value. The peak values relationship between the 1.020 µm and 0.382/0.500 µm is 0.675. Using this relationship the peak value of estimated ΔLWDN flux anomaly would be 0.675 * (-6 Wm^{-2}) = -4.05 Wm^{-2}. The ΔLWDN is been estimated to follow AT signal of Mauna Loa.

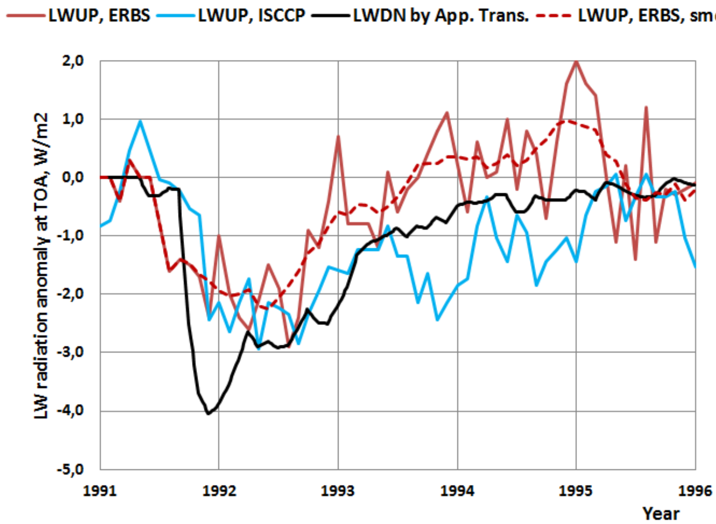

Fig. 6. LW radiation flux anomalies at TOA.

Another way to estimate the peak value of LWDN anomaly is to assume that the ΔLWUP flux at TOA is reflected in the same way as the total sun irradiation is reflected back to the space because of the eruption aerosols. The percentage of the ΔSWIN anomaly is -6 Wm^{-2} /342 Wm^{-2} = -1.75 %. Using this same percentage the LWDN anomaly would be -0.0175 * 239 Wm^{-2} = -4.2 Wm^{-2}. This value is close to the estimated value above. The estimated ΔLWDN flux is depicted in Fig. 7.

In Fig. 7 it can be noticed that its peak value is much larger than the ΔLWUP values measured at TOA by ISCCP and by ERBS. One explanation is that ΔLWUP fluxes depend mainly on the surface temperature and therefore there is a dynamic delay in comparison to the ΔLWDN flux. The full effect of this delay is about one year. In the dynamic situations like this Pinatubo eruption anomaly, the maximum temperature anomaly is about from 80 to 90 % from the full effect. This difference is analyzed more deeply in the simulation section.

In the simulations the measured surface temperature anomaly ΔT is a reference. There are five dataset commonly available and four of them are depicted in Fig. 7. [5], [38]-[40]. There are small differences in the trends. The UAH MSU trend has the largest minimum value during the eruption. Because of this situation, two surface temperature trends have been used as references namely Tmsu (UAH MSU dataset) and Tav (average of four datasets).

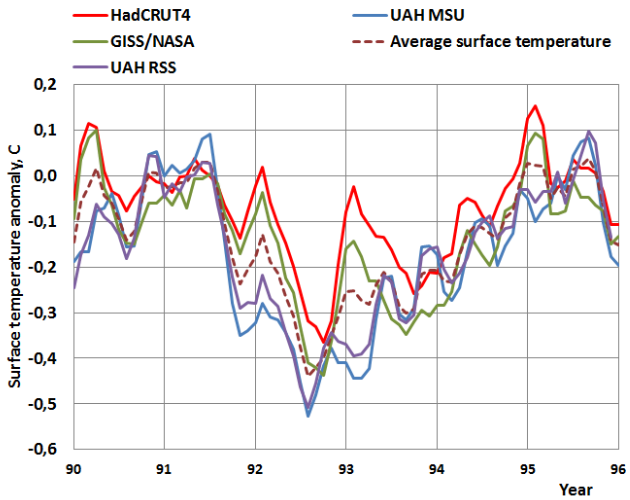

Fig. 7. Surtace temperature anomalies according to four datasets.

Hansen et al. [22] and Soden et al. [23] have taken into account that the ENSO (El Niño Southern Oscillation) phenomenon had the maximum warming index in January 1992, when the Pinatubo eruption had the strongest cooling effects. So the researchers elimated the ENSO effect by calculating a modified surface temperature of MSU UAH dataset. According to the graphs of these two papers, the ENSO corrected minimum peak of ΔT has been from -0.7 ℃ to -0.75 ℃. They refer to the study of Santer et al. [41]. The author reads this same paper that the maximum mean volcanically induced cooling ΔT_{max} at the surface is from -0.35 ℃ to -0.45 ℃ and it is about double in the troposphere. ENSO certainly has a warming effect from 1991 to the end of 1992, and therefore this result is not logical, because the temperatures without ENSO corrections are about the same. There is a graph [41], where the temperature anomaly is about -0.75 ℃ but it is for the troposphere and not for the surface. Another study of Thompson et al. [42] shows the maximum warming effect of ENSO only 0.14 ℃.

Because the effects of ENSO are so controversial, this study has used the results of the own analyses. The elimination of ENSO is based on the analysis of ONI values (Oceanic Niño Index) [43] and the global ΔT values. The ENSO effect creates fluctuations, which can be identified as almost identical fluctuations of ΔT values after 1-12 months delay. The four most regular El Niño / La Niña cases were selected. The relationship from peak to peak between these fluctuations show that ΔT = 0.144 * ΔONI in average. These two relationships have been used in modifying the measured ΔT values. In Fig. 8 is depicted the ENSO effect as a temperature anomaly and its effect on the two global ΔT trends. This approach gives the maximum ENSO effect of about 0.2 ℃. The ENSO during the Pinatubo eruption has a special feature not having the negative La Niña temperature peak at all.

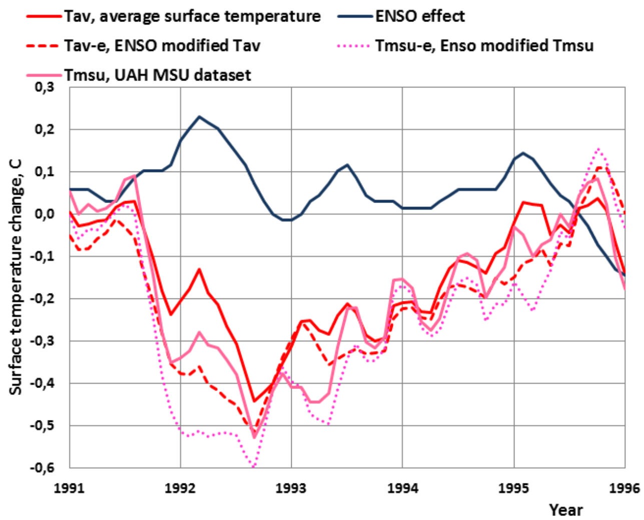

Fig. 8. The ENSO signal removed from the surface temperature measurement.

The ENSO effect explains quite well, why there is a peak upward, when the surface temperature should be in minimum because of forcing by ΔSWIN/ΔLWDN anomaly. After 1993 the ENSO effect is very small but it caused an upward tick at the end of 1995, when the Pinatubo event was practically over. The ENSO modified surface temperatures Tav-e and Tmsu-e have been used as references in this study.

3. DYNAMIC MODEL SIMULATIONS

The Pinatubo eruption happened in such a way that the forcing factors in the form of ΔSWIN and ΔLWDN flux anomalies changed all the time, and therefore the applied model must be dynamical. A dynamical model is capable of simulating time dependent variables and their impacts. In this case a simple one dimensional model 1DDM has been applied as described in Fig. 9. The 1DDM has been written in Laplace domain, because it is the most common and easiest way to describe dynamic processes.

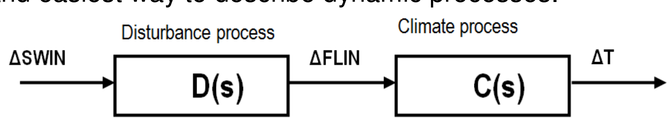

Fig. 9. The dynamic simulation model of the climate system.

Three different simulation cases have been described and carried out: 1) ΔSWIN and ΔLWIN fluxes are from ERBS datasets, 2) ΔSWIN and ΔLWIN are estimated as described above based on the AT measurements, 3) Feedback process experiment. The ISCCP dataset turned out to be too swaying and unreliable and therefore it has not been used. In cases 1) and 2) the simulations have been carried out by λ values of 0.27 $K/(Wm^{-2})$ and 0.5 $K/(Wm^{-2})$.

The input variable ΔSWIN is a flux anomaly signal varying according to the time. The output ΔFLIN of the disturbance process D(s) are ΔSWIN and ΔLWDN fluxes delayed by 1.6 months. In the case of ERBS, the ΔLWDN is replaced by ΔLWUP anomaly flux. The ΔSWIN and ΔLWDN fluxes are summarized and multiplied by the λ, which transforms the radiative flux forcing at TOA into the temperature change ΔT at the surface. The flux ΔFLIN is the product of this operation. Therefore the C(s) contains only the time delays of the climate system.

The climate process C(s) is a combination of two parallel processes, which are the dynamic processes of land and ocean:

$$C(s) = K_{sea}/(1+T_{sea}) + K_{land}/(1+T_{land}), \qquad (2)$$

where K_{sea} is 0.7, K_{land} is 0.3, T_{sea} is a time constant of 2.74 months and T_{land} is a time constant of 1.04 months. These values are based on the earlier studies [11], [44]-[45]. The values of the K parameters are the area portions of land and ocean of the Earth.

The dynamic processes according to eq. (2) are first-order dynamic models, which can be simulated in the discrete form enabling continuously changing input variables:

$$Out(n) = (\Delta t/(T+\Delta t))((T/\Delta t)*(Out(n-1)+In(n)), \qquad (3)$$

where Out(n) is the output of the process in step n, In(n) is the input of the process of step n, T is the time constant, Δt is the simulation step interval (=0.2 months), and n-1 is the previous step value.

The results of using ERBS flux values are depicted in Fig. 10.

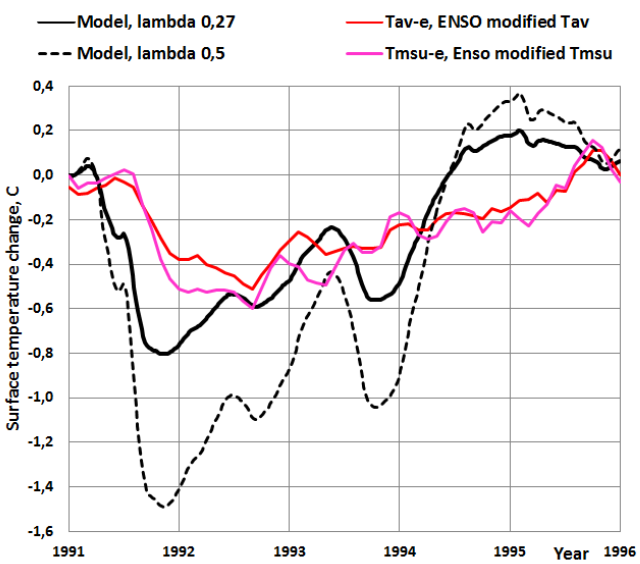

Fig. 10. The simulated surface temperature according to the dynamic 1DDM using ERBS dataset ΔSWIN and ΔLWUP fluxes.

It can be noticed that the simulated temperature values vary a lot because the fluxes ΔSWIN and ΔLWIN vary too much. Especially the λ value of 0.5 $K/(Wm^{-2})$ gives ΔTm peak values, which are almost double as large as the ΔTm values using the λ value of 0.27 $K/(Wm^{-2})$. A possible reason for this is that the LWUP flux anomaly is not an accurate enough estimate of the real ΔLWDN flux anomaly and the flux measurements are too inaccurate.

The GCM simulations of Soden et al. [23] gave rather different results. The reasons are that 1) the ΔLWDN was on a much smaller change (-4 Wm^{-2}versus -5.5 Wm^{-2} of this study), and 2) the large fluctuations of ΔLWDN flux after January 1993 were smoothed out and the

ΔLWDN flux was forced to the zero level around March 1993. Researchers did not explain these choices. If the same choices would have made in this study, the minimum ΔTm would be about -0.6 ℃ and the 1DDM-predicted ΔTm after 1993 would be very close to the observed values with the λ-value of 0.27 K/(Wm^{-2}).

In Fig. 11 the same graphs are depicted, when the ΔSWIN and ΔLWDN are estimated according to AT measurements. The simulated ΔTm signal is stable and the dynamic changes follow very well the real temperature changes ΔT. Also in this case the λ value of 0.5 K/(Wm^{-2}) gives results, which do not follow the real changes of the surface temperature changes but gives too great ΔTm during the first 1.5 years of the eruption..

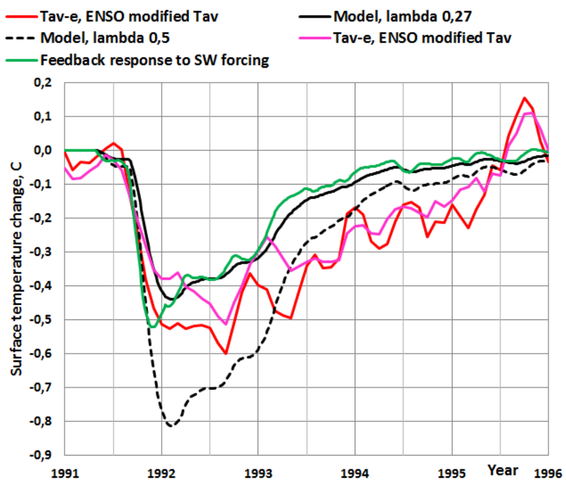

Fig. 11. The simulated surface temperature according to the dynamic 1D model using estimated SWIN and LWDN fluxes.

The question of feedback has created the two schools of thoughts. Some researchers think that the climate system is like the other processes of the nature, which are built on negative feedbacks. A positive feedback system is dangerous, because it drives any system out of balance sooner or later. IPCC and some other researchers think that the climate system for example includes the positive water feedback as well as positive albedo and cloud feedbacks [28]. It should be noticed that the positive water feedback is included into the climate feedback parameter λ, when its value is 0.5 K/(Wm^{-2}) [26]. The λ-value of 0.27 K/(Wm^{-2}) means a constant water content of the atmosphere.

A theoretical feedback process is simulated using the process model depicted in Fig. 12.

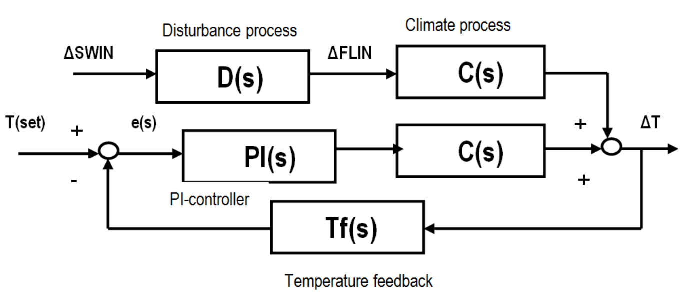

Fig. 12. A theoretical feedback process in the case of Pinatubo eruption.

The theoretical feedback process can be constructed based on the assumption that the ΔSWIN flux anomaly is the only disturbance in a very stable climate system, which tries to eliminate this disturbance. The elimination process is a theoretical PI-controller, which detects a change in the surface temperature and creates an eliminating phenomenon, which tries to minimize the disturbance. In this case the eliminating flux is the ΔLWDN flux. The climate process C(s) has as an input only the ΔSWIN anomaly. The PI-controller imitates the counter effect of ΔLWDN flux but ΔLWDN flux values are not needed to use in this simulation.

The mathematical form of the PI-controller in Laplace domain is

$$Out(s) = K_p(1+1/(T_i s))e(s) \qquad (4)$$

Where K_p is the gain of the controller, T_i is the integral time and e(s) is the error signal between the set point and the measurement. The equation (4) simulated in a discrete form in the time domain is

$$Out(t) = K_p{}^* \Delta e(t) + (K_p/T_i)\Sigma e(t)\Delta t \qquad (5)$$

The PI-controller was tuned by trial and error giving K_p = 2 and T_i = 500 months. The results of the negative feedback process simulation are depicted in Fig. 11. The 1DDM-predicted ΔTm follows surprisingly closely the ΔTm values of simulation as well the measured and ENSO corrected ΔT values using the λ values of 0.27 K/(Wm^{-2}).

One big difference between this study and the three referred studies [20], [22], and [23] is the use of estimated ΔLWDN instead of measured ΔLWUP fluxes. The basic reason is that these two fluxes have different values. The measured ΔLWUP fluxes are not stable making the results very unstable, too. This problem can be eliminated to a certain degree by heavy smoothing or even by removing parts of a flux signal [23].

The actual ΔLWUP flux depends on the surface temperature changes ΔT which is caused by the RF change. The RF is the sum of ΔSWIN+ΔLWDN flux changes. The ΔLWUP flux can be calculated using the measured ΔT changes. The author has used two calculation methods. The first is MODTRAN radiation code available through Internet [46]. By applying the average global atmosphere profile, MODTRAN can calculate the LWUP flux change at TOA. The main parameters selected for these calculations were: CO_2 357 ppm, fixed water vapor pressure, cloudy sky with cumulus cloud base of 0.66 km and top of 2.7 km. The 1 ℃ change in the surface temperature gives ΔLWUP change of 3.39 Wm^{-2} for the clear sky and 3.08 Wm^{-2} for the cloudy sky at TOA. By combining the two sky conditions, the all-sky value of 3.18 can be calculated [10]. Ollila [10] has calculated the same relationship using another commercial spectral analysis tool Spectral Calculator for the clear sky conditions. The cloudy sky fluxes are estimated to be 25 % less than the clear sky fluxes [28]. This calculation method gives the ΔLWUP change of 3.05 Wm^{-2} for the 1 ℃ change. The results of MODTRAN calculation have been used, which gives a linear relationship

$$\Delta LWUP = 3.18 * \Delta T. \qquad (6)$$

This linear relationship is applicable inside the small temperature change of 1 ℃.

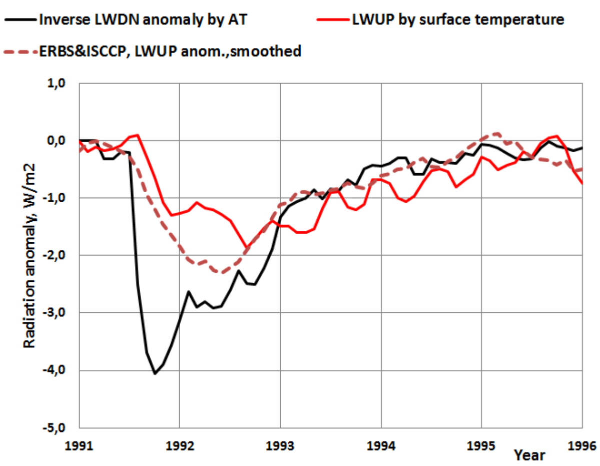

Fig. 13. The LW fluxes during the Pinatubo eruption.

The surface temperature calculated ΔLWUP is depicted in Fig. 13. It can be compared to the measured ΔLWUP flux, which is in this case the average of ISCCP and ERBS datasets. The observed flux has a minimum, which is about three months earlier than the 1DDM-predicted minimum. Anyway this is a very good result showing that ΔLWUP depends on ΔSWIN +ΔLWDN fluxes and their dynamic effects on the ΔT at the Earth's surface. Therefore ΔLWUP is not really the right choice in calculating the surface temperature changes caused by downward radiation flux anomalies of SWIN and LWDN.

4. CONCLUSION

The results show that a simple one dimensional dynamic model 1DDM gives results that are close to the real surface temperature changes ΔT after the Mount Pinatubo eruption using the climate sensitivity parameter value of 0.27 K/(Wm^2). Timewise the changes follow very well the real changes. It means that the applied time constants for land (1.04 months) and for ocean (2.74 months) are accurate and can be used in any dynamic simulations. Especially the quick and large ΔT during the early phase of the eruption shows that the applied 1DDM follows very accurately the real change rate.

The maximum temperature decrease differs +0.07 ° from lowest dataset value (HadCRUT4) and -0.09 ℃ from the highest dataset value (UAH MSU) being actually in the middle of the dataset changes. This is a very good accuracy taking into account that the difference between the different temperature datasets is in its maximum 0.16 ℃ during the minimum peak of the eruption.

The climate sensitivity parameter value of 0.5 K/(Wm^2) gives the minimum peak value of -0.82 ℃, which is almost double in comparison to λ value of 0.27 K/(Wm^2). This means that the climate models are very sensitive to the value of the climate sensitivity parameter. The mean λ-value of 1.0 K/(Wm^{-2}) commonly used in GCMs would give 200 % too high values.

In this study ΔSWIN and ΔLWDN fluxes have also been estimated utilizing the apparent transmission measurements. The simulation using these fluxes gives the best and consistent results. The theoretical feedback simulation gives values which are close to the 1DDM model values applying the ΔLWDN flux values.

The theoretical simulation of negative feedback of the climate system gives ΔTm results, which follow well both the 1DDM results and the real ΔT measurements.

5. DISCUSSION

These results can be compared to the results calculated by Hansen et al. [22] and Soden et al. [23] who have used complicated GCMs in their analyses. In these models the temperature effects are based on the eruption aerosol amounts and properties. When comparing the dynamic behavior, the calculated ΔTm of GCMs follows very accurately the real temperature change as does the 1DDM. The conclusion is that the dynamical time delays in their GCMs must come very close to the time constants applied in this study.

The peak values of ΔTm of the GCM studies are -0.6 °C [22] and -0.7 °C [23] and according to their graphs, the model-predicted values are practically same as the observed values. The observed values of the GCM studies are almost twice as large as used in this study (ΔTm = -0.44 °C). One explanation is that in GCM studies a modified UAH MSU dataset has been used, which seems to have a greater ENSO effect correction than is this study.

In the GCM calculations the researchers have used ERBS flux values. In both cases the maximum value of SW anomaly ΔSWIN has been about -4 Wm^{-2}, which differs 33 % from the value of -6 Wm^{-2} used in the majority of the other GCM studies and also in this study. The maximum LW anomaly ΔLWUP used in the GCM studies has been about -2.5 Wm^{-2}. Using eq. (1) for steady-state conditions, the calculated peak ΔT would be 0.5 * (-4 + 2.5) = -0.75 °C. This value is very close to the model-predicted value of Soden et al. [23]. On the other hand, if the commonly used value of -6 Wm^{-2} were to be used, the calculated peak ΔT would be 0.5 *(-6 + 2.5) = -1.75 °C. Because the average λ-value of GCMs is 1.0 K/(Wm^{-2}) the ΔT would be even larger.

This simple analysis shows that the model-predicted ΔTm values are completely depending on the selected forcing fluxes and even on the selected observed ΔT value. It looks that in GCM simulations [22]-[23] the selected ΔSWIN flux cannot be regarded as the justifiable choice. Actually the greatest uncertainty is about the right ΔLWDN flux values, because there are no direct measurements available. The commonly used ΔLWUP flux as a part of radiative forcing at TOA, is not the same flux as ΔLWDN. ΔLWUP is mainly depending on the real RF fluxes and on the surface temperature. Therefore it contains for example the dynamic delays of the land and ocean and finally the warming effects of the forcing radiation fluxes. In the dynamic simulations this is a source of error. The real measured ΔLWDN fluxes are very spiky – especially ISCCP fluxes.

6. REFERENCES

1. Russel PB, Livingston JM, Pueschel RF, Bauman JJ, Pollack JB, Brooks SL, et al. Global to microscale evolution of the Pinatubo volcanic aerosol derived from diverse measurements and analyses. Journal of Geophysical Research. 1996;101:18745-18763.
2. Gu L, Baldocchi DD, Wofsy SC, Munger JW, Michalsky JJ, Urbanski SP, Boden TA. Response of a deciduous forest to the Mount Pinatubo eruption. Science. 2003; 299:2035-2038.
3. Farquhar GD, Roderick ML. Pinatubo, diffuse light and the carbon cycle. Science. 2003;299:1997-1998.
4. Stowe LL, Carey RM, Pellegrino PP. Monitoring the Mount Pinatubo aerosol layer with NOAA-11 AVHHR Data. Geophysical Research Letters. 1992;19:159-162.
5. UAH MSU temperature dataset. http://www.nsstc.uah.edu/data/msu/
6. Apparent transmission dataset at Mauna Loa. Available: http://www.esrl.noaa.gov/gmd/webdata/grad/mloapt/mlo_transmission.dat

7. Wild M, Gilgen H, Roesch A, Ohmura A, Long CN, Dutton EG, et al. From dimming to brightening: decadal changes in solar radiation at Earth's surface. Science. 2005;308:847-850.
8. Minnis P, Harrison EF, Stowe LL, Gibson GG, Denn FM, Doelling DR, Smith WL. Radiative climate forcing by the Mount Pinatubo eruption. Science. 1993;259:1411-1415.
9. Raschke E, Kinne S, Stackhouse PW. GEWEX Radiative Flux Assessment (RFA). December 2012, WCRP Report No. 19/2012.
10. Ollila A. Earth's energy balance for clear, cloudy and all-sky conditions. Development in Earth Science. 2013;1:September.
11. Ollila A. Dynamics between clear, cloudy and all-sky conditions: cloud forcing effects. Journal of Chemical, Biological and Physical Sciences. 2013;4:557-575.
12. Stenchikov GL, Kirchner I, Robock A, Graf H-F, Antuna JC, Grainer RG, et al. Radiative forcing from the 1991 Mount Pinatubo volcanic eruption. Journal of Geophysical Research. 1998;103:13837-13857.
13. Kirchner I, Stenchikov GL, Graf H-F, Robock A, Antuna JC. Climate model simulation of winter warming and summer cooling following the 1991 Mount Pinatubo volcanic eruption. Journal of Geophysical Research. 1999;104:19039-19055.
14. Graf H-F, Kirchner A, Robock A, Schylt I. Pinatubo eruption winter climate effects. Model versus observations. Climate Dynamics. 1993;9:81-93.
15. Ramachandran S, Ramaswamy V, Stenchikov GL, Robock A. Radiative impact of the Mount Pinatubo volcanic eruption: Lower stratospheric response. Journal of Geophysical Research. 2000;105:409-424.
16. Yang F, Schlesinger ME. On the surface and atmospheric temperature changes following the 1991 Pinatubo volcanic eruption: A GCM study. Journal of Geophysical Research. 2002;107:4073.
17. Thomas MA. Simulation of the climate impact of Mt. Pinatubo eruption using ECHAM5. Dissertation at Hamburg University 2008.
18. Forster F, Collins M. Quantifying the water vapour feedback associated with post-Pinatubo global cooling. Climate Dynamics. 2004;23:207-214.
19. Kelly PM, Jones PD, Pengqun J. The spatial response of the climate system to explosive volcanic eruptions. International Journal of Climatology. 1996;16:537-550.
20. Hansen J, Lacis A, Ruedy R, Sato M. Potential climate impact of Mount Pinatubo eruption. Geophysical Research Letters. 1992;19:215-218.
21. Timmreck C, Graf H-F, Kirchner I. A one and a half year interactive MAECHAM4 simulation of Mount Pinatubo aerosol. Journal of Geophysical Research. 1999;104:9337-9359.
22. Hansen J, Sato M, Ruedy R, Lacis A, Asamoah K, Borenstein S, et al. A Pinatubo climate modelling investigation. NATO ASI Series. 1996;I:233-272.
23. Soden BJ, Wetherald RT, Stenchikov GL, Robock A. Global cooling after the eruption of Mount Pinatubo: A test of climate feedback by water vapor. Science. 2002;296:727-730.
24. Vonder Haar TH, Bytheway JL, Fortsyth JM. Weather and climate analyses using improved global water vapor observations. Geophysical Research Letters. 2012;39:L16802, doi:10.1029/2012GL052094.
25. NVAP dataset. NCEP/NCAR Reanalysis. Available: http://www.esrl.noaa.gov/psd/data/timeseries/
26. IPCC. Climate response to radiative forcing. IPCC Fourth Assessment Report (AR4), The Physical Science Basis, Contribution of Working Group I to the Fourth Assessment Report of the Intergovernmental Panel on Climate Change, Cambridge University Press, Cambridge. 2007.
27. IPCC. Climate Change 2001 – IPCC Third Assessment Report. The Physical Science Basis. Contribution of Working Group I: The Scientific Basis. Radiative Forcings of Climate Change Contents. Cambridge University Press, Cambridge; 2007.

28. IPCC. The Physical Science Basis. Working Group I Contribution to the IPCC Fifth Assessment Report of the Intergovernmental Panel on Climate Change, Cambridge University Press, Cambridge. 2013.
29. Ollila A. The potency of carbon dioxide (CO_2) as a greenhouse gas. Development in Earth Science.2014;2:20-30.
30. Aldrin M. Holden M, Guttorp P, Bieltvedt Skeie R. Myhre G, Koren Berntsen GT. Bayesian estimation on climate sensitivity based on a simple climate model fitted to observations of hemispheric temperature and global ocean heat content. Environmetrics. 2012;23: 253-271.
31. Bengtson L, Schwartz SE. Determination of a lower bound on earth's climate sensitivity. Tellus B. 2012. htpp://dx.doi.org/10.3402/tellub.v65i0.21533
32. Lewis NJ. An Objective Bayesian Improved Approach for Applying Optimal Fingerprint Techniques to Estimate Climate Sensitivity. Journal of Climate. 2013;26:7414-7429.
33. Otto A, Otto FEL, Boucher O, Church J, Hegeri G, Piers M, et. al. Energy budget constraints on climate response. Nature Geoscience. 2013;6:415-416. http://dx.doi.org/10.1038/ngeo1836.
34. Harde, H. Advanced two-layer climate model for the assessment of global warming by CO_2. Open Journal of Atmospheric and Climate Change. 2014;1:1-50.
35. Lindzen RS, Yong-Sang C. On the observational determination of climate sensitivity and its implications. Asia-Pacific Journal of Atmospheric Sciences. 2011;47:377-390.
36. ISCCP radiation fluxes. Available: http://isccp.giss.nasa.gov/products/products.html
37. ERBS radiation fluxes. Available: https://eosweb.larc.nasa.gov/project/erbe/erbe_table
38. HadCRUT4 temperature dataset. Available: https://eosweb.larc.nasa.gov/project/erbe/erbe_table
39. GISS/NASA temperature dataset. Available: http://data.giss.nasa.gov/gistemp/tabledata_v3/GLB.Ts+dSST.txt
40. UAH RSS temperature dataset. Available: http://data.remss.com/msu/monthly_time_series/RSS_Monthly_MSU_AMSU_Channel_TLT_Anomalies_Land_and_Ocean_v03_3.txt
41. Santer BD, Wigley TML, Doutriaux C, Boyle JS, Hansen JE, Jones PD, et al. Accounting for the effects of volcanoes and ENSO in comparisons of modelled and observed temperature trends. Journal of Geophysical Research. 2001;106:28033-28059.
42. Thompson DWJ, Wallace JM, Jones PD, Kennedy JJ. Identifying signatures of natural climate variability in time series of global-mean surface temperature: Methodology and insights. Journal of Climate. 2009;22:6120-6141.
43. NOAA Oceanic Nina Index – ONI. Available: http://www.cpc.ncep.noaa.gov/products/analysis_monitoring/ensostuff/ensoyears_1971-2000_climo.shtm
44. Stine AR, Huybers P, Fung IY. Changes in the phase of the annual cycle of surface temperature. Nature. 2009;457:435-441.
45. Kauppinen J, Heinonen JT, Malmi PJ. Major Portions in Climate Change: Physical approach. International Review of Physics. 2011;5:260-270.
46. MODTRAN radiation code. Available: http://climatemodels.uchicago.edu/modtran/